RSC Advances

PAPER

View Article Online
View Journal | View Issue

Cite this: *RSC Adv.*, 2023, **13**, 29270

Synthesis of PVP-capped trimetallic nanoparticles and their efficient catalytic degradation of organic dyes

Kanwal Memon,*[a] Roomia Memon,*[ab] Awais Khalid,*[c] Bader S. Al-Anzi,[d] Siraj Uddin,[e] Syed Tufail Hussain Sherazi,[a] Answer Chandio,[a] Farah Naz Talpur,[a] Asma Abdul Latif[f] and Iram Liaqat[g]

The study proposes a simple and efficient way to synthesize a heterogeneous catalyst that can be used for the degradation of organic dyes. A simple and fast chemical process was employed to synthesize Au: Ni: Co tri-metal nanohybrid structures, which were used as a catalyst to eliminate toxic organic dye contamination from wastewater in textile industries. The catalyst's performance was tested by degrading individual dyes as well as mixtures of dyes such as methylene blue (MB), methyl orange (MO), methyl red (MR), and Rose Bengal (RB) at various time intervals. The experimental results show the catalytic high degradation efficiency of different dyes achieving 72–90% rates in 29 s. Moreover, the material displayed excellent recycling stability, maintaining its degradation efficiency over four consecutive runs without any degradation in performance. Overall, the findings of the study suggest that these materials possess efficient catalytic properties, opening avenues toward their use in clean energy alternatives, environmental remediation, and other biological applications.

Received 31st May 2023
Accepted 6th August 2023

DOI: 10.1039/d3ra03663d

rsc.li/rsc-advances

1. Introduction

Water contamination is caused by various hazardous pollutants originating from pharmaceutical drugs, insecticides, and steroid hormones, and other industries. One of the most dangerous discharges of organic dyes comes from textile industries during different dyeing steps. The dyes waste is at least 5% and can reach up to 50% depending upon the dye and type of fabric in use. As a result of this, around 200 billion liters of colored effluents are yearly generated.[1,2] In addition to that, hair color[3] and leather tanning,[4,5] the food industry, as well as the paper industry, also contribute to the discharge of dye in water. This can cause lethal effects such as genotoxicity, mutagenicity, and carcinogenicity to humans and living organisms.[6] In the future, it is estimated that the world will face a major water crisis due to different reasons. Due to the above-mentioned facts, scientists turned their attention to the possibility of treating industrial wastewater effluents with dyes and exploring innovative treatment methods. Many methods have been reported in the literature previously such as microbial degradation,[7] photo-catalytic degradation,[8–17] flocculation,[18] activated carbon sorption,[19] redox treatment,[20] electro-coagulation, *etc.* All the reported methods are expensive, ineffective, and time-consuming and the generation of by-products is the main drawback of using these methods. Therefore, to provide healthy reformative/wholesome remediation, a non-toxic eco-friendly method, a single-step nanomaterials approach has been developed.[21] Metal nanoparticles are classified as monometallic, bimetallic, trimetallic and so on, based on the number of metallic components. When metal nanoparticles are mixed, they usually exhibit new or stronger properties that differ from the ones held by their original components. This is why researchers have recently concentrated on trimetallic nanoparticles.[1,2] Trimetallic nanoparticles are of importance due to their higher outstanding catalytic performance in association with the single metal or BNPs.[3] The development of multimetallic core–shell or alloy nanoparticles has gained significant attention in recent decades both from the fundamental and application perspectives.[4,5] Trimetallic nanoparticles have established increased research awareness in recent years due to their new chemical and physical properties derived from the synergistic effects of their components. Trimetallic nanoparticles are desirable in technical applications,

[a]*National Centre of Excellence in Analytical Chemistry, University of Sindh, 76080, Pakistan. E-mail: kanwalmemon51@yahoo.com; roomiamemon99@gmail.com*
[b]*Sabanci University, SUNUM Nanotechnology Research and Application Center, Tuzla, 34956, Istanbul, Turkey*
[c]*Department of Physics, Hazara University Mansehra, Khyber Pakhtunkhwa 21300, Pakistan*
[d]*Department of Environmental Technologies and Management, Kuwait University, P.O. Box 5969, Safat 13060, Kuwait*
[e]*HEJ Research Institute of Chemistry, International Centre for Chemical and Biological Sciences, University of Karachi, 75270, Pakistan*
[f]*Department of Zoology, Lahore College for Women University, Lahore 54000, Pakistan*
[g]*Microbiology Lab, Department of Zoology, Government College University, Lahore 54000, Pakistan*

particularly for catalytic processes. These nanoparticles were synthesized using different methods, including microwave, co-precipitation, hydrothermal, selective catalytic reduction, and microemulsion.

We demonstrate here that trimetallic Au: Ni: Co NPs with dendritic alloy type well defined morphology which can be synthesized in a high yields by a facile aqueous by following one step synthetic method with no need templates. The co-reduction of multiple precursors of different metals has been carried with single reducing agent (aspirin) strong enough to gave a fine control over the growth kinetics and nucleation resulting in formation of Au: Ni: Co NPs.

Furthermore, the prepared NPs showed excellent catalytic activity and stability for the electrooxidation of aqueous media.

2. Materials and methods

2.1 Materials

Hydrogen tetrachloroauratetrihydrate ($HAuCl_4 \cdot 3H_2O$), cobalt II chloride ($CoCl_2 \cdot 6H_2O$) and nickel chloride ($NiCl_2 \cdot 6H_2O$) from sigma Aldrich, polyvinylpyrrolidone (PVP), sodium borohydride ($NaBH_4$), sodium hydroxide (NaOH) from Fischer Chemical HK limited, Nafion NR50 was purchased from Sigma-Aldrich, USA, KOH, methylene blue (MB), methyl red (MR), methyl orange (MO) and Rose Bengal (RB) dyes were purchased from E. Merck, all the foregoing chemicals and reagents used in this work were of analytical grade and directly used without further purification. Stock solutions were prepared by dissolving the appropriate amount of each salt according to concentration. Throughout experimental work, Mili Q water was used.

2.2 Instrumentation

The nanocrystalline structure was studied using X-ray Diffraction (XRD) by a Philips PW 1729 diffractometer using CuKα. A Fourier transform infrared technique (FTIR) was applied to find out interaction of TNPs with the capping agents. UV-vis spectra were recorded by using Cary Series UV-vis spectrophotometer (Cary 100 UV-vis). Atomic force microscopy and Scanning electron microscopy (SEM) is used to verify the size and morphology of synthesized trimetallic nanoparticles. Elemental composition was confirmed by EDS.

2.3 Synthesis of PVP capped Au–Ni–Co TNPs

The strategy of Au–Ni–Co TNPs is straightforward as indicated by different ratios of each metal *i.e.* ($Au_{0.5}Ni_2Co_1$), here subscripts show the corresponding ratio of the metals that were added in 15 mL vial, then 100 μL of PVP was added. After stirring for 5 minutes, about 100 μL of $NaBH_4$ as a reducing agent was added for reduction purposes. By adding $NaBH_4$ light pink color appears that, after stirring for 10 minutes, changes to dark black Fig. 1.

2.4 Catalysis study of PVP-capped Au: Ni: Co TNPs in the reduction of dyes

Degradation of dyes was carried out by synthesized PVP capped TNPs, these particles were found to be the best catalyst for various organic dyes. To investigate the catalytic activity of Au–Ni–Co TNPs, various dyes were selected such as methylene blue (MB), Rose Bengal (RB), methyl orange (MO), methyl red (MR) and the mixture of all four dyes were measured in the presence and absence of nanoparticles along with sodium borohydride ($NaBH_4$). Real water samples such as textile industrial wastewater were also checked. 0.4 mL of 100 μM of each dye was taken in the cuvette and diluted up to 4 mL followed by the insertion of 0.5 mL of 0.01 M of $NaBH_4$ and observed the degradation with changing absorbance by UV-visible spectrophotometer.

2.5 Reduction of different organic dyes

The catalytic activity of synthesized PVP capped Au–Ni–Co TNPs was checked against the reduction of organic dyes such as Methylene blue (MB), Rose Bengal (RB), methyl orange (MO), and methyl red (MR) in the present as well as without $NaBH_4$. Nanocatalyst was added to the test solution of each dye having 10 μM concentration with 10 mM of $NaBH_4$ and the reduction process was monitored using UV-visible spectroscopy. Various parameters were optimized like the concentration of NPs and $NaBH_4$. The test was performed in a standard 1.0 cm^3 quartz cuvette having 1 cm path length. For observation of the catalytic activity of the prepared nanocatalyst, about 1 mL of TNPs was added to the solution of dyes. All the factors such as concentration and amount of TNPs, organic dyes, and $NaBH_4$ were optimized according to the best results obtained.[22]

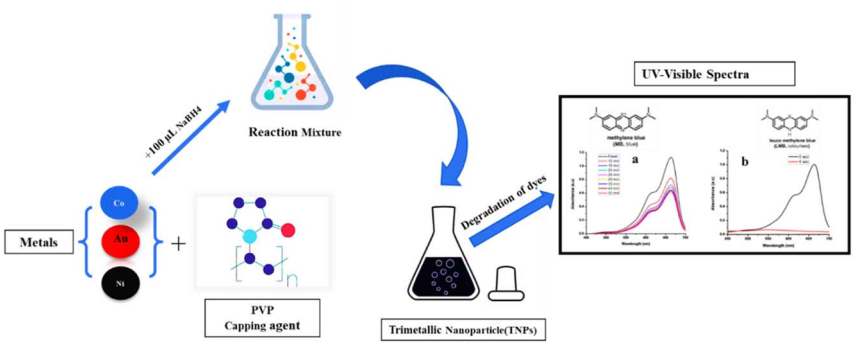

Fig. 1 Schematic diagram for illustration of complete process (synthesis to dye degradation).

2.6 Procedure for reduction of all the four dyes

For reduction of dyes, 10 μM of MB was added along with 0.5 mL of $NaBH_4$ in a quartz cuvette, then 1 mL (0.1 mg) of prepared nano catalyst was poured in that cuvette. The following parameters volume of $NaBH_4$, nanoparticles amount and concentration of dyes were optimized according to optimized conditions. By adding Nano catalyst to the dye solution color disappears within seconds, and UV-visible spectra were observed.

3. Results and discussion

3.1 UV-visible spectroscopy

UV-visible absorption spectroscopy is the basic techniques to confirm the formation of nanoparticles to get the stable and small monodisperse nanoparticles. The colloidal dispersion of Au–Ni–Co TNPs was prepared by mixing three metal precursors simultaneously in the presence of PVP as a capping agent and $NaBH_4$ as a reducing agent. The UV-vis spectra of the dispersion of the Au–Ni–Co TNPs show an absorption peak around 600 nm as well as those of the Au, Ni, Co monometallic and, Au–Co, Au–Ni, and Ni–Co BNPs as shown in fig. 2.

3.2 pH study of synthesized trimetallic nanoparticles

The UV-visible spectra in Fig. 3 clearly demonstrate the Surface Plasmon Resonance (SPR) of PVP-capped trimetallic nanoparticles over a pH range from 3 to 7. Notably, the SPR absorption is visibly present for all pH values within this range but at pH 5, the enhancement of SPR absorption indicates the complete reduction and stability of the synthesized nanoparticles, with relatively small in size at approximately 57 nm. This stable and small particle size of PVP-TNPs at pH 5 makes them ideal for further investigation as an efficient photocatalyst for dye degradation. The results show that the photodegradation of the dye substantially increases with an increase in pH value, reaching its highest efficiency at pH ~5, within the acidic pH range. This behavior can be attributed to the effect of pH on the absorption behavior and surface charge properties of the catalyst. Might be at higher pH levels, the catalyst surfaces become more negatively charged, leading to improved decolorization of the dye. These findings indicates the promising potential of the PVP-capped trimetallic nanoparticles for efficient and environmentally friendly dye degradation applications respectively.

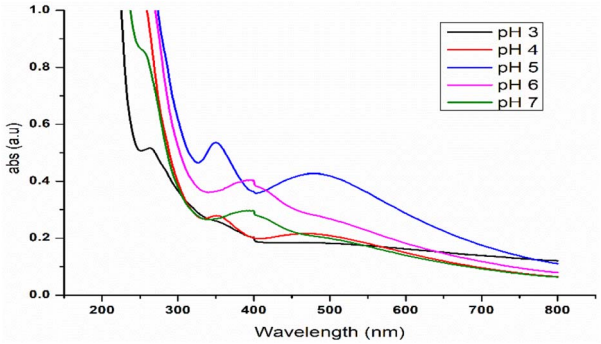

Fig. 3 pH study response of synthesized trimetallic nanoparticles.

3.3 FT-IR analysis

Fourier transform infrared spectroscopy is well-known technology to investigate the interaction of a functional group of capping agents with metals. Furthermore, FTIR spectroscopic studies verify attachment of specific functional group through shift, appearance and disappearance of FTIR signal which confirms the attachment of particular functional group in the reaction mixtures compared with non-interactive functional group. Fig. 4a and b shows PVP and PVP capped TNPs, by comparing both the spectra it is observed that a broad peak between 1288 and 1655 cm^{-1} in spectra (a) which relate to C–N stretching motion and C=O stretching motion of monomer for PVP and absorption peaks at 1495–1466, 1371 cm^{-1} are accredited to C–H bonding respectively.[23] In spectra (b) there is a decrease in intensity of the peak in the range of 1288–1644 cm^{-1} and 1495–1466, 1371 cm^{-1} occurs that confirms the interaction of nitrogen of PVP to the synthesized TNPs.

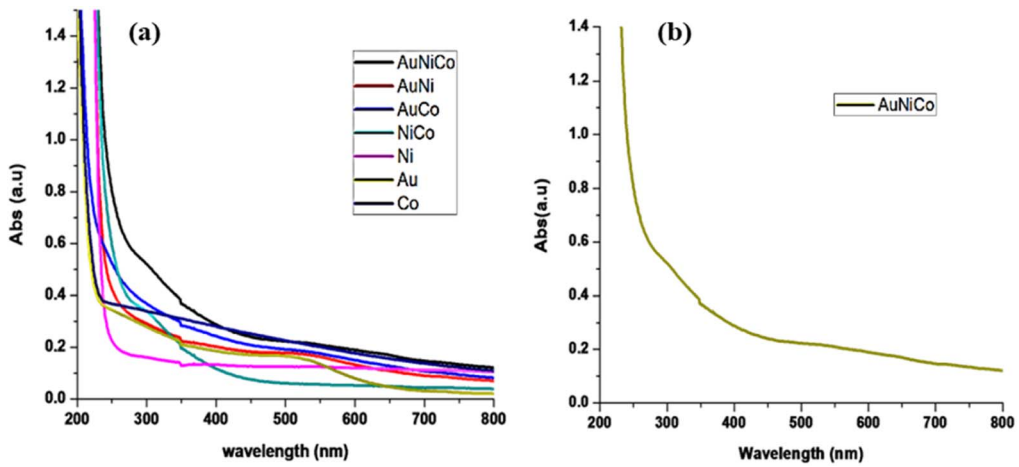

Fig. 2 (a) Different combinations of metal nanoparticles (b) UV-visible spectra of selected combinations of metals Au–Ni–Co.

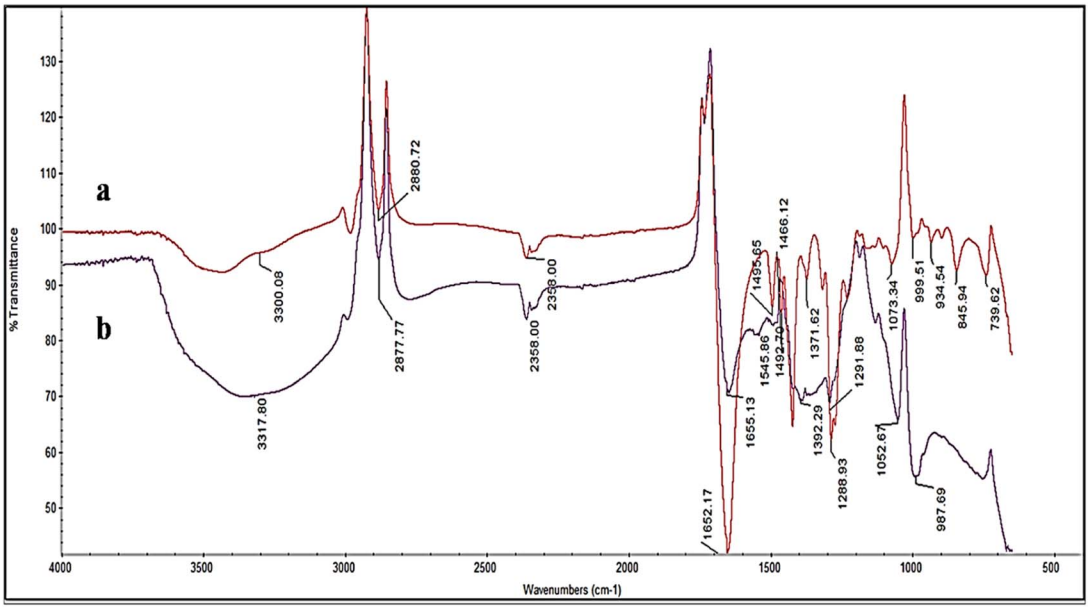

Fig. 4 FTIR spectra of (a) Polyvinylpyrrolidone (PVP) (b) PVP capped TNPs.

3.4 Energy dispersive spectroscopic study

The energy dispersive spectroscopy (EDS) analysis of the synthesized trimetallic nanoparticles (TNPs) confirms the presence of specific metals in the sample. The EDS spectrum reveals the presence of Gold (Au), Nickel (Ni) and Cobalt (Co) elements in the TNPs. Importantly, the atomic ratio of these metals, as determined from the EDS data, is found to be approximately 2.59 : 8.6 : 4.68, which shows good agreement with the expected or appointed atomic ratio of 2 : 8 : 4 for the TNPs. In addition to the metals, the EDS analysis also identifies the presence of other elements in the sample. These elements are attributed to the capping agent used during the synthesis of the TNPs, which in this case is polyvinylpyrrolidone (PVP). The elements identified in PVP include carbon (C), nitrogen (N), and oxygen (O), respectively. This comprehensive EDS characterization not only confirms the successful synthesis of the desired trimetallic nanoparticles with the specified metal composition but also validates the presence of the capping agent and its associated elements in the sample. These findings further support the understanding of the TNPs' structural and compositional properties, which are crucial for their catalytic performance and potential applications Fig. 5.

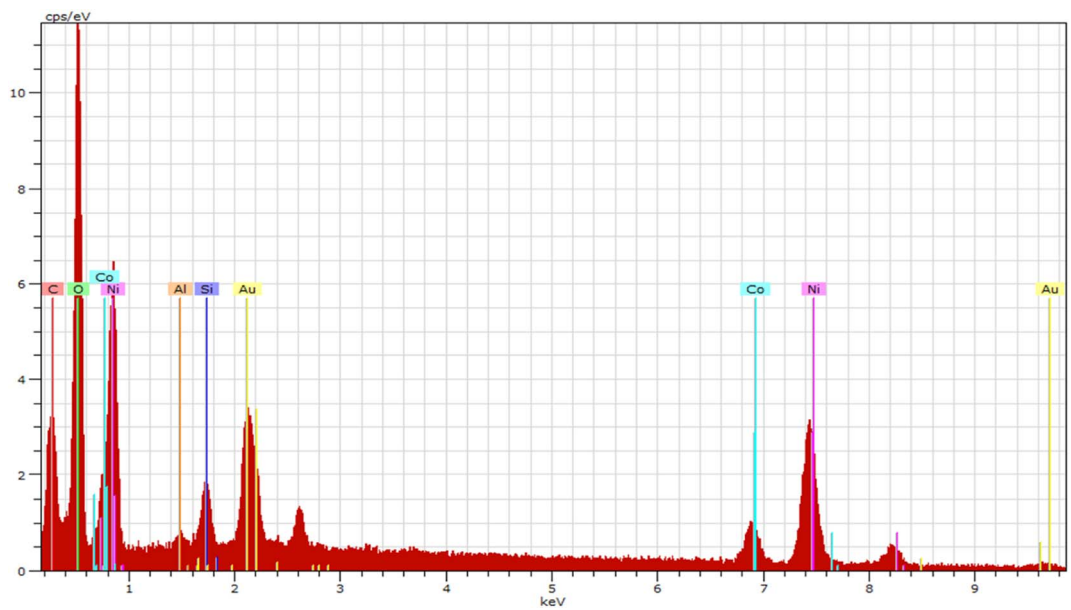

Fig. 5 EDS spectra of PVP capped TNPs.

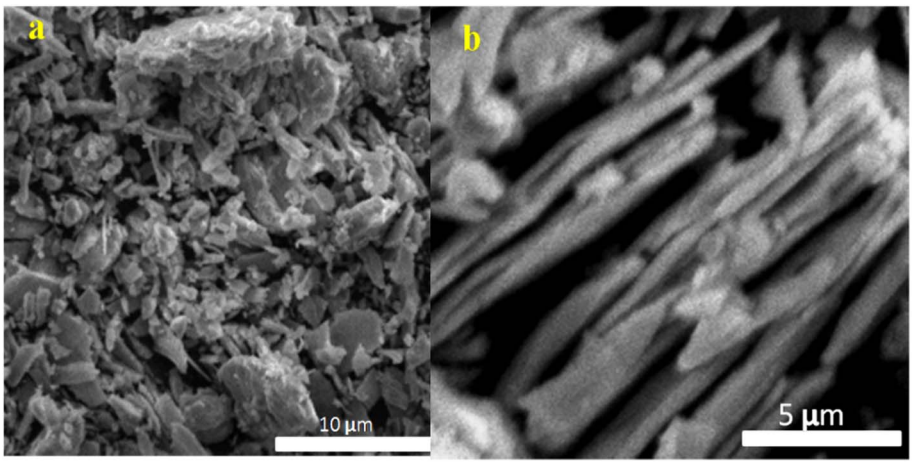

Fig. 6 (a) SEM images of PVP-capped TNPs at low resolution (b) PVP-capped TNPs at high resolution.

3.5 Scanning electron microscopy analysis

The SEM images of the prepared sample reveal intriguing structural features of the synthesized trimetallic nanoparticles (TNPs) at low resolution (Fig. 6a), the TNPs exhibit a bead-like structure, while at high resolution (Fig. 6b), they display rod-like structures. These distinct morphologies are of particular interest for catalytic applications, as they offer increased surface area and potentially provide additional active sites, enhancing the catalytic activity. Furthermore, the slightly rough surface and sharp edges observed in the TNPs are characteristic of nanoparticles, which are highly advantageous for catalysis. Such surface properties facilitate more efficient interaction between the nanocatalyst and reactants, thereby promoting catalytic reactions. These structural characteristics are particularly beneficial for catalytic processes, as they not only supports the catalytic activity but also ease the removal of the nanocatalyst upon the completion of the catalytic reaction. This feature is crucial for recycling and reusing the nanocatalyst, making it more environmentally sustainable and economically viable for various catalytic applications. Overall, the SEM observations provide valuable insight into the unique structural attributes of the synthesized TNPs, which hold promising potential for advancing catalytic processes and their practical applications.

3.6 Atomic force microscopy (AFM)

The AFM images provide valuable insights into the surface morphology and size characteristics of the prepared nanoparticles. In Fig. 7a, it is evident that some of the particles exhibit a spherical shape and are well-dispersed (monodispersed), indicating uniformity in size and shape. On the other hand, certain particles display a bead-like morphology, suggesting some variation in their structures within the sample. In Fig. 7b, the average diameter of the synthesized PVP-TNPs is measured to be approximately 57 nm. This finding gives us a crucial understanding of the nanoparticles' size distribution, highlighting their nanoscale dimensions. The combination of AFM imaging and diameter analysis contributes significantly to our comprehension of the

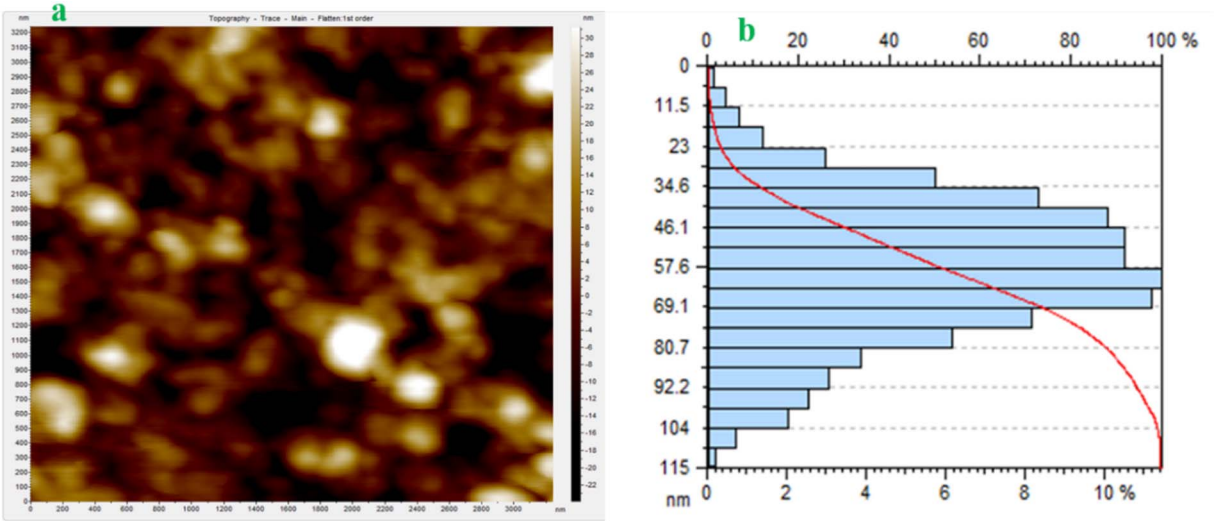

Fig. 7 (a) AFM image of PVP-capped trimetallic nanoparticles (TNPs), (b) the average diameter of the synthesized PVP-TNPs.

nanomaterial's surface properties and size characteristics. These observations are vital in evaluating the potential catalytic performance and other applications of the synthesized PVP-TNPs, making them a promising candidate for various nanotechnology-based endeavors.

3.7 X-ray diffraction spectroscopy

The X-ray diffraction (XRD) analysis of the PVP-capped TNPs is illustrated in Fig. 8. The XRD diffractogram for the Au–Ni–Co TNPs exhibits distinct peaks at 38.50°, 44.66°, 64.81°, and 77.5°, which can be indexed to the (111), (200), (220), and (311) crystal planes, respectively, of a face-centered cubic (FCC) structure. Comparing the observed peaks with literature data for Ni–Co bimetallic nanoparticles, it is found that the expected peaks should appear at 2θ values of 44.3°, 51.5°, and 76.2°, corresponding to the (111), (200), and (220) crystal planes. However, in the XRD pattern of the Au–Ni–Co TNPs, the peaks at 51.5° and 76.2° are absent, and there is a right shift of these peaks. This right shift and absence of peaks at 51.5° and 76.2° are attributed to the presence of Gold (Au) in the synthesized TNPs. The shift and absence of these peaks in the XRD pattern confirm the formation of Au–Ni–Co trimetallic nanoparticles, indicating successful incorporation of Au into the Ni–Co bimetallic structure. XRD analysis provides strong evidence of the crystalline structure of the synthesized nanoparticles and confirms the successful formation of the desired Au–Ni–Co TNPs, underscoring their potential for catalytic and other applications.

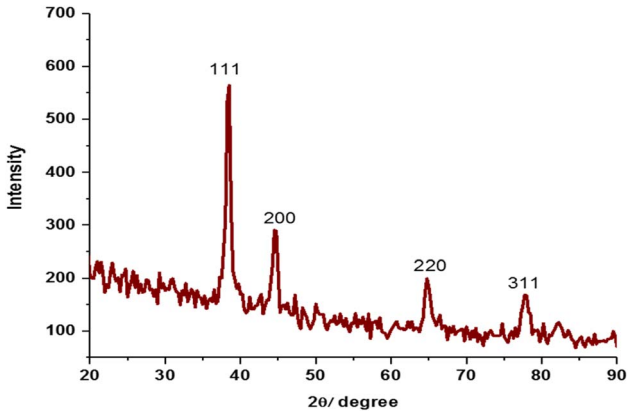

Fig. 8 XRD diffractogram of PVP capped TNPs.

3.8 Reduction of methylene blue (MB)

In order to determine the catalytic activity of prepared TNPs for degradation of methylene blue (basic cationic dye) in an aqueous solution.[24] In aqueous medium MB shows an absorption band at 664 nm with a shoulder at 614 nm.[23] Degradation was observed in the presence of a strong reducing agent *i.e.*, $NaBH_4$ as well as in the presence of TNPs along with a reducing agent. As it is shown in results the rate of reaction comparatively slow for reduction of methylene blue in the presence of a reducing agent ($NaBH_4$). Whereas, when TNPs nanocatalyst were introduced along with $NaBH_4$, there was a significant increase in the degradation of methylene blue observed. This enhanced catalytic activity of the prepared TNPs can be seen in Fig. 9b, where the absorption peak at 664 nm (associated with MB) promptly disappeared. The degradation of MB resulted in the formation of a colorless leucomethylene blue product indicating the successful breakdown of the dye molecule within 5 s.[25]

3.9 Reduction of methylene red (MR)

Discharge of organic dyes from textile industries is the major source of water pollution. Methyl red is also the main water pollutant of wastewater and needs to be removed from the water stream.[24] Methyl red (MR) is a commonly used monoazo dye in laboratory assays, textiles, and other commercial products. It may

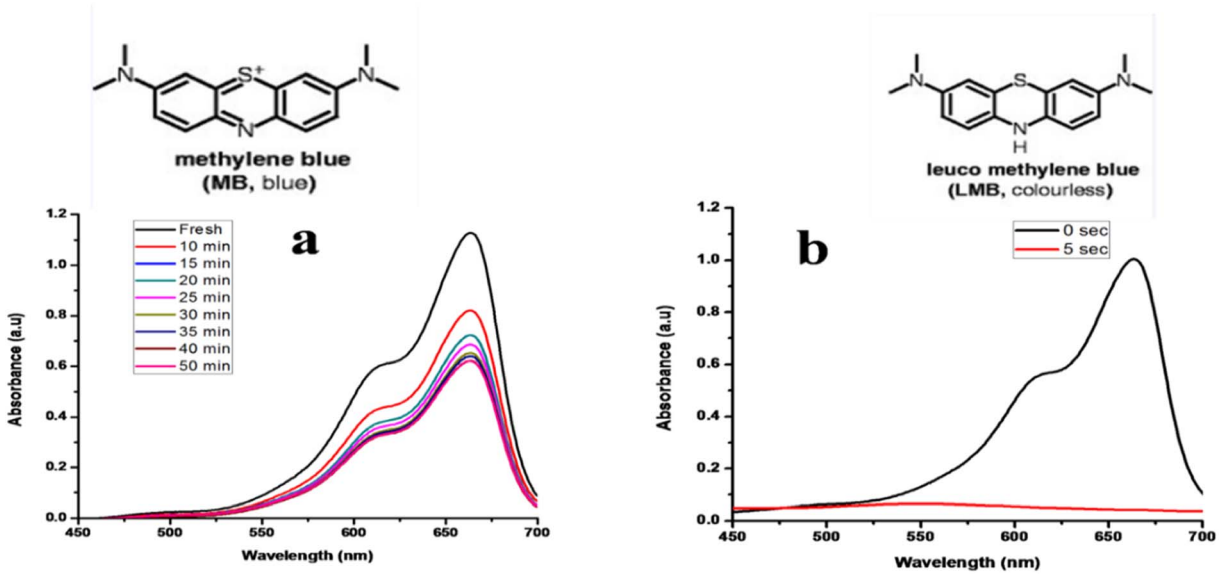

Fig. 9 (a) Reduction of methylene blue dye in the absence of TNPs (b) With TNPs.

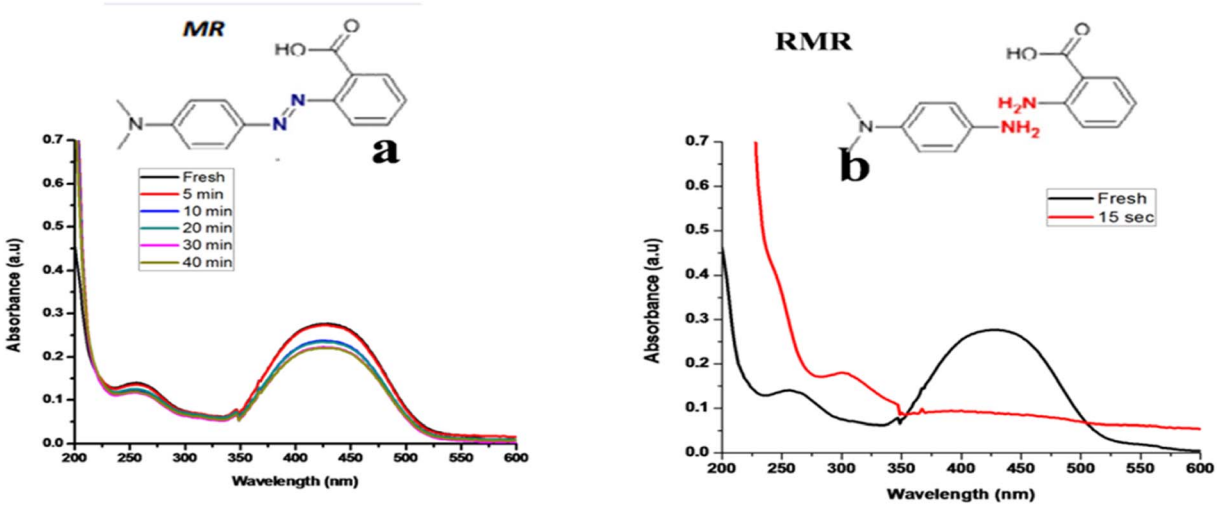

Fig. 10 Degradation of methyl red (a) in the absence of TNPs (b) in the presence of TNPs.

cause eye and skin sensitization and digestive tract irritation if inhaled or swallowed.[26] Fig. 10 shows the degradation of methyl red in the absence as well as the presence of TNPs and it was observed that in the absence of TNPs degradation occurs very slowly and up to 21% in 40 min, while in the presence of catalyst along with reducing agent rate of reaction was very fast, peak at lambda max 426 rapidly disappears and 70% of dye degraded completes within 15 s.

3.10 Reduction of methyl orange dye (MO)

MO is commonly used as azo dye and it is also present in wastewater of industries. Maximum absorption of methyl orange appears at 463 nm. From Fig. 11a and b it can be observed that in the presence of a strong reducing agent, only 21% of dye was degraded up to 40 min, and by adding TNPs degradation of dye occurs very fast *i.e.*, 71% of dye degraded within only. It shows great catalytic activity for synthesized TNPs.

3.11 Reduction of Rose Bengal (RB)

Rose Bengal dye which is commonly known as (4,5,6,7-tetrachloro-2′,4′,5′,7′-tetraiodofluorescein) is extensively used in the printing, insecticides and dying industries.[27] Rose Bengal dye shows the maximum absorption at 547 nm in an aqueous solution. Reduction of dye was carried out in the presence of $NaBH_4$ which is the strongest reducing agent and based on Fig. 12, very little degradation was achieved *i.e.*, 34% occurred up to 40 min. By adding TNPs in the presence of reducing agent 91% degradation occurs only within 10 s.

3.12 Simultaneous reduction of mixture of dyes

In simultaneous reduction, a mixture of all four dyes was taken in equal amounts and degradation was observed by using UV-vis spectrophotometry. From Fig. 13 it was observed that in the presence of TNPs, 83% of a mixture of dyes was degraded within only 29 s respectively.

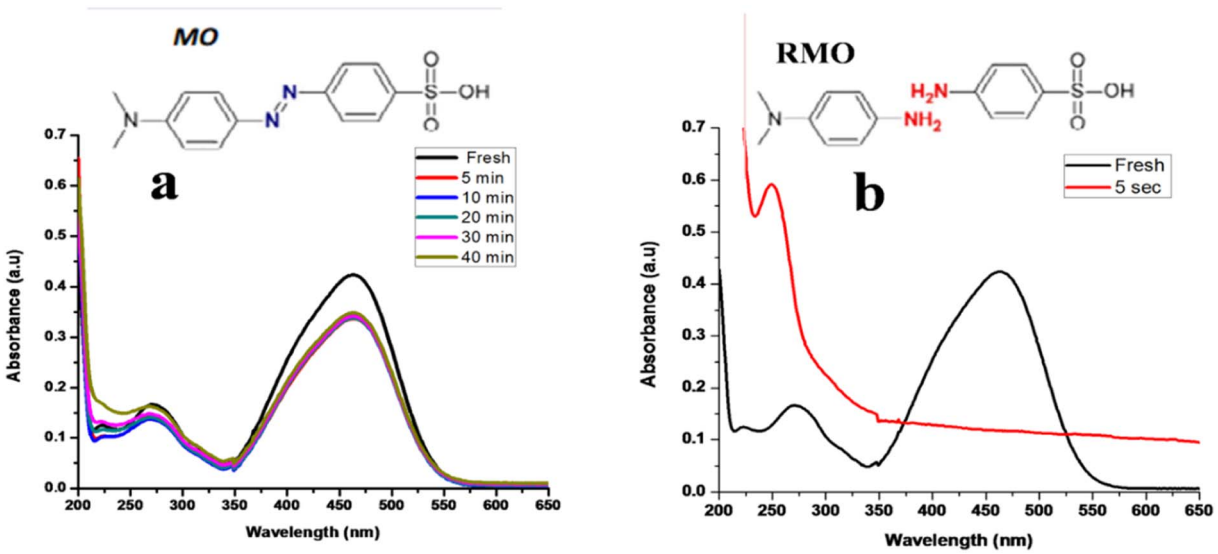

Fig. 11 Degradation of methyl orange (a) without TNPs (b) with TNPs.

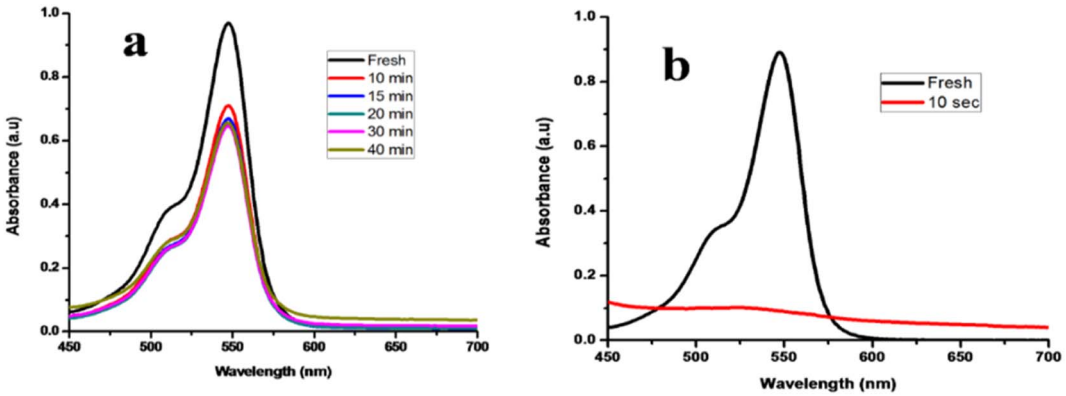

Fig. 12 Degradation of Rose Bengal (a) in the absence of TNPs (b) in the presence of TNPs.

3.13 Industrial wastewater samples

The catalytic activity of TNPs was examined by degrading real wastewater dye-containing samples. Real wastewater samples were collected from drains of three different local textile industries in Karachi. Catalytic degradation was performed with a similar methodology as mentioned above, with an optimized amount of TNPs 1 mL (0.1 mg) and 0.5 mL of 100 mM ($NaBH_4$) reductant and 10 μL of real sample diluted up to 0.4 mL with deionized water. Fig. 14 shows UV-vis spectra for the reductive degradation of real samples. Complete degradation was observed in a very short reaction time indicating the highly efficient nature of Au–Ni–Co TNPs.

3.14 Degradation mechanism

In this photocatalytic process as illustrated in Fig. 15, it is assumed, that a possible mechanism for the degradation of carcinogenic organic dyes over trimetallic nanocatalyst in the presence of UV-visible light radiation. When light applied to the reaction mixtures light-induced electron and hole is exist over trimetallic nanoparticles with O_2 and OH to form oxidant $^{\bullet}O_2$ and $^{\bullet}OH^{-}$, respectively, then it react with organic compounds and degrade them. In the trimetallic nanoparticles increased oxygen valances are accountable for the degradation process by the mechanism of chemical wet oxidation (CWO). This mechanism is described previously by.[28–31]

4. Discussion

The catalyst efficiency was checked by different concentrations of dyes concentrations ranging from 1–10 μM used to access the maximum photocatalytic activity while keeping other variables constant. Fig. 9–15 shows degradation and mechanism of methyl orange (MO), methyl red (MR), Rose Bengal (RB) and mixture of these dyes and textile waste water treatments. It is revealed in figures without the catalyst degradation rate was comparatively too slow and it takes time in mins with lowest percentage 45% of degradation. But after the addition of nanocatalyst, it was degraded within seconds with 96% degradation was achieved. Moreover, The percent degradation was also checked at different amounts of catalyst by keeping other experimental conditions constant. The degradation percentage of dyes by different catalyst doses, 0.1–1 g L^{-1} for 10 μM concentration of dyes such as methyl orange, methyl red, Rose Bengal and a mixture of these dyes was examined. It is may be due to the reason of with increases in the concentration of dyes interference from intermediates formed upon degradation of parental dye molecules for that reason suppression would be more pronounced in the presence of high percent degradation intermediates formed upon an increased dye concentration.[32,33] Furthermore, the contact time of dyes with the catalyst is an important parameter that influence the catalytic degradation process regardless of the

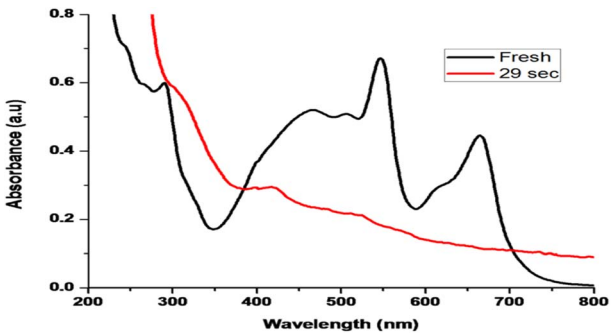

Fig. 13 Degradation of a mixture of four different dyes.

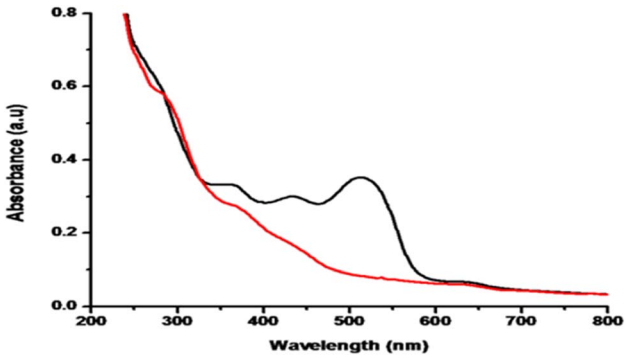

Fig. 14 UV-visible spectra for reductive degradation of real sample.

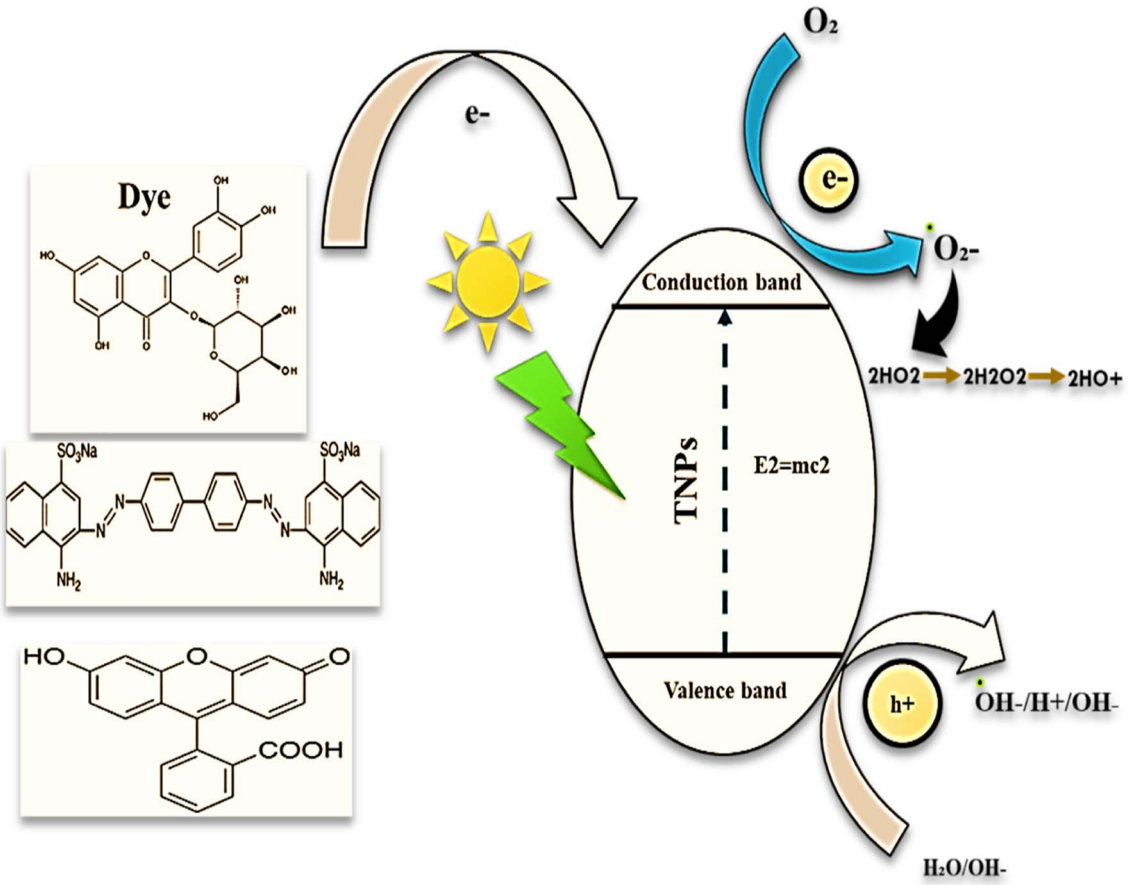

Fig. 15 Mechanism of degradation of dyes organic dyes from textile samples.

type of catalyst generally, as the reaction time increases the decomposition rate increases by keeping other parameters constant. As it is discussed in previous report in Fenton process varied the reaction time from 30 to 120 min and observed that with the passage of time COD increased with disappearance of the colour of dye catalytic percentage achieved 45–69%.[34] Another reported work discussed by Karthikeyan *et al.* also observed after the addition of homogeneous/heterogenous catalyst it took 4 h for complete removal of dyes with maximum percent degradation.[35,36] During current work, catalytic degradation of organic dyes *via* PVP-Au: Ni: Co nanocatalyst, it is concluded 98% removal of methyl orange, methyl red, Rose Bengal and a mixture of dyes obtained after addition with just 0.1 mg of catalyst gives immediate degradation 80–90% within sec respectively.[37] It is revealed in the Fig. 9–15 as the amount of the catalyst increases the particle-to-particle interaction also increases this is the major factor to reduce light absorption by the photocatalyst. Also, the agglomerations prevent photons from reaching the inner layers of the catalyst so the minimum quantity is sufficient to achieve maximum degradation.[37] Hence, the least amount of catalyst particles gets excited and ultimately lower number of electron/holes and hydroxyl radicals were produced. Therefore, the degradation rate tends to decrease as the catalyst dose increases.[38]

4.1 Comparative study

Table 1 shows comparative study of combination of different trimetallic nanoparticles and their catalytic applications. In 2004, Pt–Ru–Co TNPs were synthesized using water-oil microemulsion with cyclohexane, Triton X-100, and 2-propanol. These nanoparticles were formed using hydrazine as a reducing agent. TEM analysis showed an average diameter of 2.7 ± 0.6 nm. It was tested as DMFC catalysts and showed improved activity due to the synergistic effects of Co and Ru with Pt. They are promising for fuel cell applications.[38] A study was conducted in 2007 by Toshima and colleagues on the synthesis of Au–Pt–Rh trimetallic nanoparticles (TNPs) with a core–shell structure. The study used polyvinylpyrrolidone (PVP) as a capping agent. The TNPs synthesized in the study showed better catalytic activity in the hydrogenation of methyl acrylate compared to both monometallic nanoparticles and bimetallic nanoparticles (BNPs).[39] Moreover, Au–Ag–Pd and Pt–Ni–Fe trimetallic nanoparticles have been studied for their exceptional catalytic performance in organic synthesis and proton exchange membrane fuel cells their potential in enhancing efficiency and performance in renewable energy technologies highlights the significance of trimetallic nanoparticles in various industrial and sustainable applications.[40] In another report a group of researchers developed Pt–Ni–Fe trimetallic nanoparticles by using three metal precursors salts and reducing them in an

Table 1 Different combinations of TNPs, their sizes, and capping/reducing agents utilized in literature

TNPs	Capping/reducing agents	Diameter size (nm)	Application	Ref.
Pt–Ru–Co	TritonX/hydrazine	2.7	Methanol oxidation	38
Au–Pt–Rh	PVP	NM	Electrocatalytic activity for ORR	39
Au–Ag–Pd	CTAB/$NaBH_4$	13.0	Methanol oxidation reaction	40
Pt–Ni–Fe	Oleylamine, oleic acid/1,2-hexadecandiol	5.3	Methanol oxidation reaction	41
Fe/Cu/Ag	$NaBH_4$	60–90	Methyl orange dye	42
Au–Ag–Pt	CTAB, ascorbic acid	NM	Immunosensor for detection of zearalenone	43
Au–Pb–Pt	PVP/$NaBH_4$, ascorbic acid	NM	NM	44
Ag–Co–Fe	PVP/ammonia borane	12.8	Dehydrogenation of amine borane	45
Ag–Ni–Fe	Methyl amine borane	19.5	Dehydrogenation of amine borane	45
Au–Pt–Pd	PVP/$NaBH_4$	2.0	MO dye degradation	47
Fe–Ni–Ce	PVP/$NaBH_4$	NM	MO dye degradation	48
Au–Ag–Cu	PVP/diethylene glycol, *N*, *N*-dimethylformamide, and ethylene glycol	NM	NM	49
Au–Pt–Ag	$NaBH_4$	1.5	Glucose oxidation	50
Cu–Fe–Ni	PVP/ammonia borane	NM	Efficient catalysts for the Heck reaction.	51
Pd–Fe–Ni	Chitin	19.54–6.27	Biotin biosensor	52
Pt–Pd–Fe	Dioctyl sulfosuccinate sodium salt/hydrazine hydrate	14–24	Efficient catalyst for reductive hydrodehalogenation of aryl and aliphatic halides	53
Au–Ni–Co	PVP	57	Degradation of multiple dyes	Current work

octyl ether solvent. These nanoparticles were then supported on carbon black and exhibited remarkable electrocatalytic activity in proton exchange membrane fuel cells. The use of these nanoparticles has the potential to enhance the efficiency of PEMFCs, making them an attractive option for sustainable energy conversion technologies.[41] Furthermore, in this article authors investigated the effectiveness of trimetallic nanoparticles Fe–Cu–Ni for breaking down methyl orange dye in water, which is commonly used in industrial processes and can lead to water contamination. Through analyzing the concentration of the dye over time, they were able to measure the catalysts' efficiency. These findings may pave the way for developing eco-friendly solutions to control water pollution and remove dyes from wastewater, Ultimately advancing sustainable water treatment methods.[42] In this experiment, Au–Pt–Ag nanocomposite and Au–Pd–Pt nanotubes were produced through microwave irradiation. UV-visible spectroscopy and high-resolution scanning electron microscopy was used to verify the existence of the TNPs nanoparticles. The outcome of this study showed that Pt was essential in enhancing the catalytic activity and structural stability of the nanoparticles. Furthermore, the use of multilayered nanoparticles provided more potential for customization and optimization of their properties to meet specific application requirements.[43,44] Meanwhile, new combination Ag–Co–Fe and Ag–Ni–Fe core–shell nanoparticles have been created with methylamine borane and graphene support. They have strong catalytic activity and can be easily dispersed on graphene. Ag@CoFe/graphene nanoparticles perform best, with excellent durability and magnetic recyclability for hydrolytic dehydrogenation of AB and MeAB. This synthesis method can be used for other metal core–shell nanoparticles supported by graphene.[45,46] Core-shell TNPs made of Cu, Fe, and Ni were synthesized through a one-step method that employed ammonia borane as a reducing agent and PVP as a capping agent. The TNPs comprising Fe–Ni–Ce and Au–Pd–Pt exhibit potential in degrading methylene blue dye.[47,48] The objective of this study was to produce Au–Ag–Cu trimetallic nanocrystals through a three-step reduction process. The addition of Cu shells to Au@Ag cores was verified by TEM, EDS, and XRD analyses. Huang and Lien *et al.* also investigated similar TNPs, using varying surfactants and catalysts.[49] Au–Pt–Ag TNPs were successfully created by Zhang and Toshima with PVP as a capping agent and $NaBH_4$ as a reducing agent. These nanoparticles exhibit an alloy structure and an average diameter of 1.5 nm. It's worth noting that they have the highest turnover frequency for aerobic glucose oxidation compared to all other metal nanoparticles that have been reported before.[50] Wang *et al.* have reported that Cu–Fe–Ni TNPs are highly effective catalysts for hydrolytic dehydrogenation of ammonia borane. Exceptional catalytic activity was observed when varying ratios of magnetic $Cu_{0.4}@Fe_{0.1}Ni_{0.5}$ NPs were utilized. In addition, TNPs have been successfully employed as a catalyst for the Hydroconversion of *n*-heptane, and for the catalysis of the Heck reaction, with the use of Au–Ag–Pd TNPs.[51] This paper presents a study concerning electrodeposition of Pd–Fe–Ni trimetallic alloy NPs by cyclic voltammetry (CV) onto a glassy carbon

electrode (GCE) modified with a room-temperature ionic liquid (RTIL)-chitin (Ch) composite film (PdFeNi/ChRTIL/GCE) aiming at BTN trace detection using differential pulse voltammetry (DPV) which has been reported for the first time. Different deposits were obtained by varying the number of cyclic potential scans during electroreduction step and we used a computerized method (DIP) for measuring PSDs. Finally the sensitivity of the best resulting Pd–Fe–Ni/ChRTIL/GCE sensor toward BTN assay was evaluated.[52] This work, provide a proper catalytic system using Pt/Pd/Fe T-NP in the HDH reaction. The activity of this novel trimetallic nano-catalyst is compared with each pair of its constituent metal elements (*i.e.*, comparison with bimetallic systems). Then, the reaction parameters are screened, and the results are evaluated. At last, the proposed reaction mechanism on Pt/Pd/Fe catalyst surface is discussed.[53]

The catalysts that was developed previously demonstrated in the above section has tremendous potential across various applications, such as the hydrolytic dehydrogenation of ammonia borane, DMF, and the hydrogenation of methyl acrylate applications. It has been proven to out perform other alternative, including monometallic and BNPs.

After conducting extensive research, we have observed that our work is groundbreaking in its utilization of a unique combination of TNPs (trimetallic nano-catalysts) that has not been previously reported. Our study showcases the application of these TNPs in catalytically degrading both single and multiple organic dyes in a matter of sec not in min. The results demonstrate the remarkable efficiency of this novel catalytic system for rapid dye degradation. This breakthrough approach offers a promising solution for remediation of dyes form contaminated water, making a significant contribution to environmental sustainability and safeguarding human health. By utilizing this innovative nanocatalyst, we have achieved faster and more efficient degradation of multiple dyes, bringing us closer to addressing textile pollution effectively and protecting our environment and well-being.

5. Conclusion

The rapid degradation observed in this study can be attributed to the exceptional adsorption capability of the nano catalyst, which facilitates the decomposition of organic molecules. To achieve this, various metal elements such as Au, Ni, Cu, Ag, and Co were employed. Among these, the combination of Au, Ni, and Co (Au: Ni: Co) proved to be the most promising. A comprehensive characterization of the synthesized Au–Ni–Co-TNPs was conducted, revealing an average diameter of 57 nm, and confirming the presence of an alloy-like composition. The synthesized Au–Ni–Co-TNPs were utilized as catalysts for the individual degradation of several organic dyes, including methylene blue (MB), Rose Bengal (RB), methyl orange (MO), and methyl red (MR). Remarkably, the degradation of all dyes occurred within a matter of seconds. Furthermore, the nano-catalyst exhibited exceptional performance in the simultaneous degradation of multiple dyes. This multi-dye degradation process was also completed within seconds, highlighting the remarkable catalytic activity of the Au–Ni–Co-TNPs. Importantly, the nanocatalyst was effectively employed for the removal of dyes from industrial wastewater, demonstrating its potential for practical applications in the treatment of contaminated water sources. Overall, the findings of this study highlight the exceptional adsorption capability and catalytic performance of the synthesized Au–Ni–Co-TNPs. The rapid degradation of organic dyes, including both individual and simultaneous degradation, underscores the potential of these nano catalysts for efficient and environmentally friendly wastewater treatment in industrial settings.

Data availability

The datasets of this manuscript are available upon request.

Conflicts of interest

The authors have no conflict of interest to declare.

References

1 T. Liu, *et al.*, Recent developments in the utilization of modified graphene oxide to adsorb dyes from water: A review, *J. Ind. Eng. Chem.*, 2023, **117**, 21–37.
2 M. Fida, *et al.*, Water contamination and human health risks in Pakistan: a review, *Exposure Health*, 2022, 1–21.
3 F. Hueber-Becker, *et al.*, Occupational exposure of hairdressers to [14C]-para-phenylenediamine-containing oxidative hair dyes: A mass balance study, *Food Chem. Toxicol.*, 2007, **45**(1), 160–169.
4 A. Cassano, *et al.*, Treatment of aqueous effluents of the leather industry by membrane processes: A review, *J. Membr. Sci.*, 2001, **181**(1), 111–126.
5 G. Crini, Non-conventional low-cost adsorbents for dye removal: A review, *Bioresour. Technol.*, 2006, **97**(9), 1061–1085.
6 M. Ismail, *et al.*, Pollution, toxicity and carcinogenicity of organic dyes and their catalytic bio-remediation, *Curr. Pharm. Des.*, 2019, **25**(34), 3645–3663.
7 S. Varjani, *et al.*, Microbial degradation of dyes: an overview, *Bioresour. Technol.*, 2020, **314**, 123728.
8 T. Tatarchuk, *et al.*, Photocatalytic degradation of dyes using rutile TiO2 synthesized by reverse micelle and low temperature methods: real-time monitoring of the degradation kinetics, *J. Mol. Liq.*, 2021, **342**, 117407.
9 A. Ajmal, *et al.*, Principles and mechanisms of photocatalytic dye degradation on TiO 2 based photocatalysts: a comparative overview, *RSC Adv.*, 2014, **4**(70), 37003–37026.
10 U. Bali, E. Çatalkaya and F. Şengül, Photodegradation of Reactive Black 5, Direct Red 28 and Direct Yellow 12 using UV, UV/H2O2 and UV/H2O2/Fe2+: a comparative study, *J. Hazard. Mater.*, 2004, **114**(1), 159–166.
11 A. Khalid, *et al.*, Structural, Optical, and Renewable Energy-Assisted Photocatalytic Dye Degradation Studies of ZnO, CuZnO, and CoZnO Nanostructures for Wastewater Treatment, *Separations*, 2023, **10**(3), 184.

12 A. Khalid, *et al.*, Biologically Reduced Zinc Oxide Nanosheets Using Phyllanthus emblica Plant Extract for Antibacterial and Dye Degradation Studies, *J. Chem.*, 2023, **2023**, 3971686.
13 A. Khalid, *et al.*, Visible-light promoted chemical fixation of carbon dioxide with epoxide into cyclic carbonates over S-scheme CdS–CeO2 photocatalyst, *Mater. Sci. Semicond. Process.*, 2023, **165**, 107649.
14 R. A. Basit, *et al.*, Successive Photocatalytic Degradation of Methylene Blue by ZnO, CuO and ZnO/CuO Synthesized from Coriandrum sativum Plant Extract *via* Green Synthesis Technique, *Crystals*, 2023, **13**(2), 281.
15 M. Hafeez, *et al.*, Synthesis of cobalt and sulphur doped titanium dioxide photocatalysts for environmental applications, *J. King Saud Univ. Sci.*, 2022, **34**(4), 102028.
16 A. Khalid, *et al.*, A practical method for incorporation of Fe (III) in Titania matrix for photocatalytic applications, *Mater. Res. Express*, 2021, **8**(4), 045006.
17 A. Khalid, *et al.*, Synthesis of Boron-Doped Zinc Oxide Nanosheets by Using Phyllanthus Emblica Leaf Extract: A Sustainable Environmental Applications, *Front. Chem.*, 2022, **10**, 930620.
18 N. Nandhini, S. Rajeshkumar and S. Mythili, The possible mechanism of eco-friendly synthesized nanoparticles on hazardous dyes degradation, *Biocatal. Agric. Biotechnol.*, 2019, **19**, 101138.
19 N. Mohammadi, *et al.*, Adsorption process of methyl orange dye onto mesoporous carbon material–kinetic and thermodynamic studies, *J. Colloid Interface Sci.*, 2011, **362**(2), 457–462.
20 P. Kumar, *et al.*, Photocatalytic degradation of methyl orange dye using silver (Ag) nanoparticles synthesized from Ulva lactuca, *Colloids Surf. B*, 2013, **103**, 658–661.
21 I. Kumar, *et al.*, Green one-pot synthesis of gold nanoparticles using Sansevieria roxburghiana leaf extract for the catalytic degradation of toxic organic pollutants, *Mater. Res. Bull.*, 2019, **117**, 18–27.
22 L. Karimi, S. Zohoori and M. E. Yazdanshenas, Photocatalytic degradation of azo dyes in aqueous solutions under UV irradiation using nano-strontium titanate as the nanophotocatalyst, *J. Saudi Chem. Soc.*, 2014, **18**(5), 581–588.
23 V. Suvith and D. Philip, Catalytic degradation of methylene blue using biosynthesized gold and silver nanoparticles, *Spectrochim. Acta - A: Mol. Biomol. Spectrosc.*, 2014, **118**, 526–532.
24 K. Jyoti and A. Singh, Green synthesis of nanostructured silver particles and their catalytic application in dye degradation, *J. Genet. Eng. Biotechnol.*, 2016, **14**(2), 311–317.
25 M. J. Plater, A degradation product of methylene blue, *Arkivoc*, 2003, **1**, 37–42.
26 B. Vinoda, *et al.*, Photocatalytic Degradation of Toxic Methyl Red Dye Using Silica Nanoparticles Synthesized from Rice Husk Ash, *J. Environ. Anal. Toxicol.*, 2015, **5**(6), 1000336.
27 S. Sharma, *et al.*, Photocatalytic degradation of Rose Bengal by semiconducting zinc sulphide used as a photocatalyst, *J. Serb. Chem. Soc.*, 2013, **78**(6), 897–905.
28 A. Srikhaow and S. M. Smith, Preparation of Cu2 (OH) 3NO3/ZnO, a novel catalyst for methyl orange oxidation under ambient conditions, *Appl. Catal. B*, 2013, **130**, 84–92.
29 Y. Huang, *et al.*, Molybdenum oxide nanorods decorated with molybdenum phosphide quantum dots for efficient photocatalytic degradation of rhodamine B and norfloxacin, *Res. Chem. Intermed.*, 2022, **48**(7), 2887–2901.
30 W. Li, *et al.*, Fast catalytic degradation of organic dye with air and MoO3: Ce nanofibers under room condition, *Appl. Catal. B*, 2009, **92**(3–4), 333–340.
31 I. Shaheen and K. Ahmad, Biomimetic Synthesis of Highly Reusable MoO3-based Catalysts for Fast Degradation of Azo Dyes, *Mater. Innov.*, 2022, **9**(10), 255–268.
32 C. Tang and V. Chen, The photocatalytic degradation of reactive black 5 using TiO2/UV in an annular photoreactor, *Water Res.*, 2004, **38**(11), 2775–2781.
33 N. M. Mahmoodi, Binary catalyst system dye degradation using photocatalysis, *Fibers Polym.*, 2014, **15**(2), 273–280.
34 S. Mohajeri, *et al.*, Influence of Fenton reagent oxidation on mineralization and decolorization of municipal landfill leachate, *J. Environ. Sci. Health A*, 2010, **45**(6), 692–698.
35 S. Karthikeyan, *et al.*, Preparation, characterizations and its application of heterogeneous Fenton catalyst for the treatment of synthetic phenol solution, *J. Mol. Liq.*, 2013, **177**, 402–408.
36 R. Javaid, *et al.*, Fabrication of microtubular reactors coated with thin catalytic layer (M=Pd, Pd–Cu, Pt, Rh, Au), *Catal. Commun.*, 2010, **11**(14), 1160–1164.
37 R. Javaid and U. Y. Qazi, Catalytic oxidation process for the degradation of synthetic dyes: an overview, *Int. J. Environ. Res. Public Health*, 2019, **16**(11), 2066.
38 X. Zhang, F. Zhang and K.-Y. Chan, Preparation of Pt–Ru–Co trimetallic nanoparticles and their electrocatalytic properties, *Catal. Commun.*, 2004, **5**(12), 749–753.
39 N. Toshima, *et al.*, Trimetallic nanoparticles having a Au-core structure, *Catal. Today*, 2007, **122**(3–4), 239–244.
40 P. Venkatesan and J. Santhanalakshmi, Synthesis, characterization and catalytic activity of trimetallic nanoparticles in the Suzuki C–C coupling reaction, *J. Mol. Catal. A: Chem.*, 2010, **326**(1–2), 99–106.
41 A. Aramata and M. Masuda, Platinum Alloy Electrodes Bonded to Solid Polymer Electrolyte for Enhancement of Methanol Electro-oxidation and Its Reaction Mechanism, *J. Electrochem. Soc.*, 1991, **138**(7), 1949–1957.
42 M. Kgatle, *et al.*, Degradation kinetics of methyl orange dye in water using trimetallic Fe/Cu/Ag nanoparticles, *Catalysts*, 2021, **11**(4), 428.
43 B. Loganathan, Rapid green synthetic protocol for novel trimetallic nanoparticles, *J. Nanopart.*, 2013, 2013.
44 M. Verma, *et al.*, Application of green nanomaterials in catalysis industry, in *Green Nanomaterials for Industrial Applications*, Elsevier, 2022. pp. 309–337.
45 L. Yang, *et al.*, Strategic synthesis of graphene supported trimetallic Ag-based core–shell nanoparticles toward hydrolytic dehydrogenation of amine boranes, *Int. J. Hydrog. Energy*, 2014, **39**(7), 3360–3370.

46 K. Aranishi, *et al.*, One-step synthesis of magnetically recyclable Au/Co/Fe triple-layered core-shell nanoparticles as highly efficient catalysts for the hydrolytic dehydrogenation of ammonia borane, *Nano Res.*, 2011, **4**, 1233–1241.

47 H. Zhang, *et al.*, Fabrication of catalytically active Au/Pt/Pd trimetallic nanoparticles by rapid injection of NaBH4, *Mater. Res. Bull.*, 2014, **49**, 393–398.

48 G. Allaedini, S. M. Tasirin and P. Aminayi, Synthesis of Fe–Ni–Ce trimetallic catalyst nanoparticles *via* impregnation and co-precipitation and their application to dye degradation, *Chem. Pap.*, 2016, **70**(2), 231–242.

49 C.-C. Huang and H.-L. Lien, Trimetallic Pd/Fe/Al particles for catalytic dechlorination of chlorinated organic contaminants, *Water Sci. Technol.*, 2010, **62**(1), 202–208.

50 H. Zhang and N. Toshima, Preparation of novel Au/Pt/Ag trimetallic nanoparticles and their high catalytic activity for aerobic glucose oxidation, *Appl. Catal., A*, 2011, **400**(1–2), 9–13.

51 P. Venkatesan and J. Santhanalakshmi, Synthesis and characterization of surfactant stabilized trimetallic Au-Ag-Pd nanoparticles for heck coupling reaction, *Phys. Chem*, 2012, **2**, 12–15.

52 M.-B. Gholivand, *et al.*, Surface exploration of a room-temperature ionic liquid-chitin composite film decorated with electrochemically deposited PdFeNi trimetallic alloy nanoparticles by pattern recognition: an elegant approach to developing a novel biotin biosensor, *Talanta*, 2015, **131**, 249–258.

53 R. Abazari, F. Heshmatpour and S. Balalaie, Pt/Pd/Fe trimetallic nanoparticle produced *via* reverse micelle technique: synthesis, characterization, and its use as an efficient catalyst for reductive hydrodehalogenation of aryl and aliphatic halides under mild conditions, *ACS Catal.*, 2013, **3**(2), 139–149.